Nuclear Parton Densities

R. Vogt

Nuclear and Chemical Sciences Division, Lawrence Livermore National Laboratory, Livermore, CA 94551, USA

Physics Department, University of California, Davis, CA 95616, USA

U.S. DEPARTMENT OF ENERGY | Office of Science

[0]This work was performed at Lawrence Livermore National Laboratory under the auspices of the U.S. Department of Energy under Contract No. DE-AC52-07NA27344.

Outline

- **Introduction to Nuclear Parton Densities**
- **Eskola *et al.* Sets, Similarities and Differences**
- **A Bit on Centrality Dependence**
- **Comparison of Results for Specific Processes**

Global Analyses of Nuclear Parton Densities (nPDFs)

Global analyses of nuclear parton densities similar to those of the proton, use same types of data except now the target is a nucleus instead of a proton

Deep inelastic scattering with nuclei showed modifications that depend on momentum fraction, momentum transfer, and nuclear mass, revealing that nucleons in the nucleus are not independent

Global analyses, different than saturation picture, assumes DGLAP evolution and addresses the entire x-range

Types of data employed in global analyses:

- nuclear deep-inelastic scattering with electrons, muons and neutrinos (not all sets have used neutrino DIS) relative to deuteron or other light target
- Drell-Yan data with initial protons (and pions in some cases)
- high p_T π^0 production from PHENIX experiment at RHIC
- latest sets from Eskola and collaborators also now employs CMS and ATLAS measurements of dijets, Z and $W^{\pm}$ from 5.02 TeV p+Pb run – new regime of high Q^2 and moderate x heretofore unavailable for nPDFs

Gluon nPDFs directly probed only by dijets and NLO contribution to gauge boson production

Some sets are available for a limited number of interesting targets but some groups have sought to make the sets available for arbitrary A

Parton Densities Modified in Nuclei

Interesting low x regime not probed for $Q^2 > 1$ GeV^2 for fixed-target energies

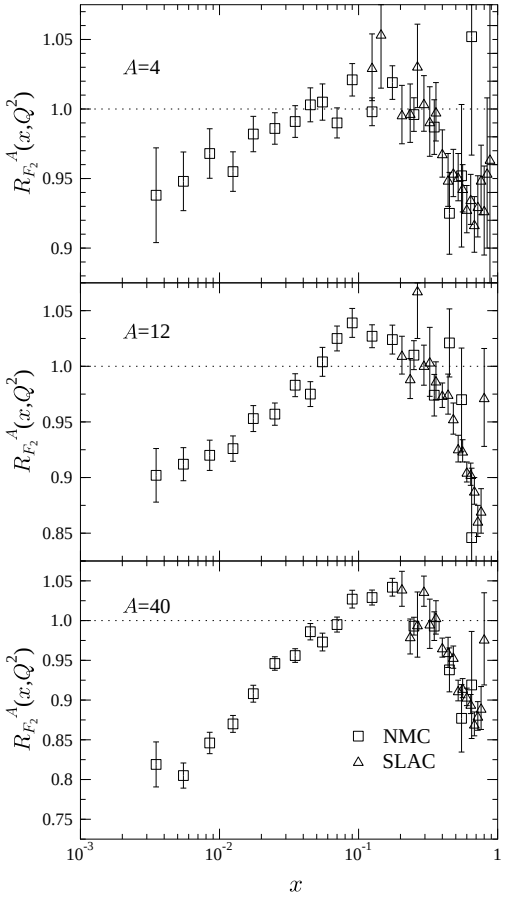

Figure 1: Ratios of charged parton densities in He, C, and Ca to D as a function of x. [From K.J. Eskola.]

Schematic View of x Dependence of nPDFs

Most nuclear parton densities assume a similar shape, the details depend on the assumptions made and the data included in the fit procedure

Amount and shape of antishadowing region depends on whether it is for valence quarks, sea quarks or gluons

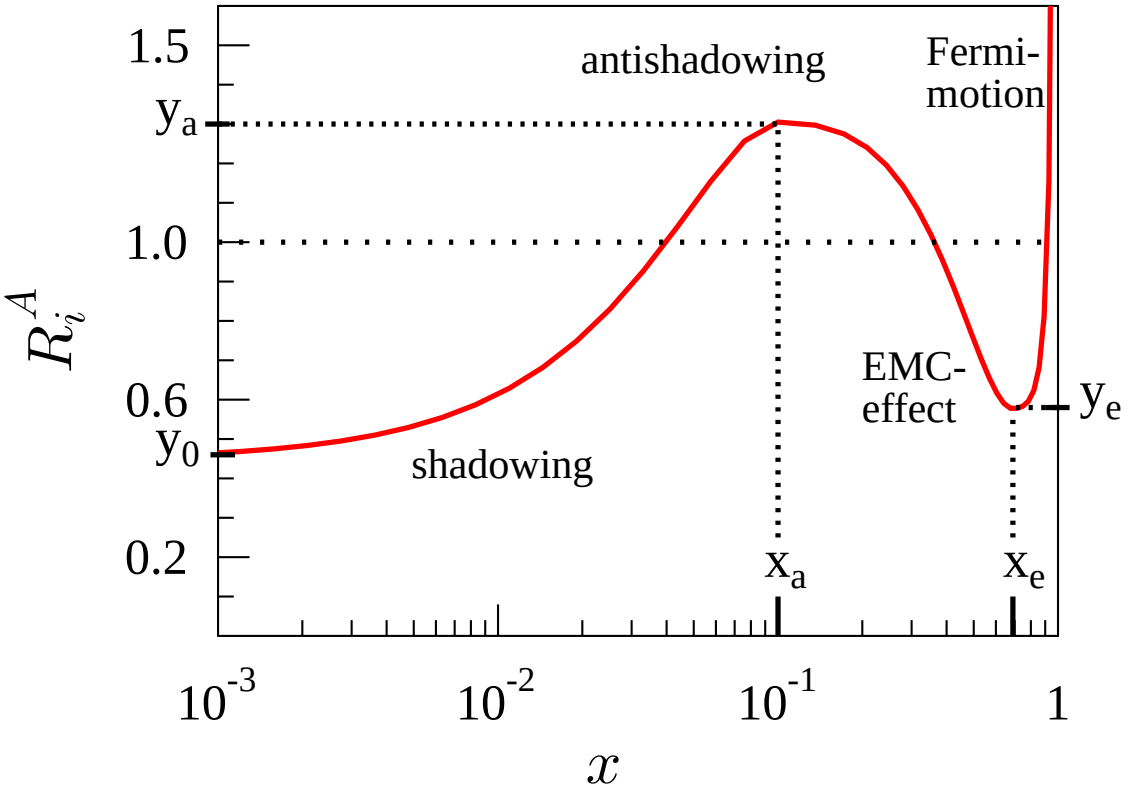

x and Q^2 Reach of Heavy Ion Colliders

Lowest x values are reached at high energies and forward rapidities

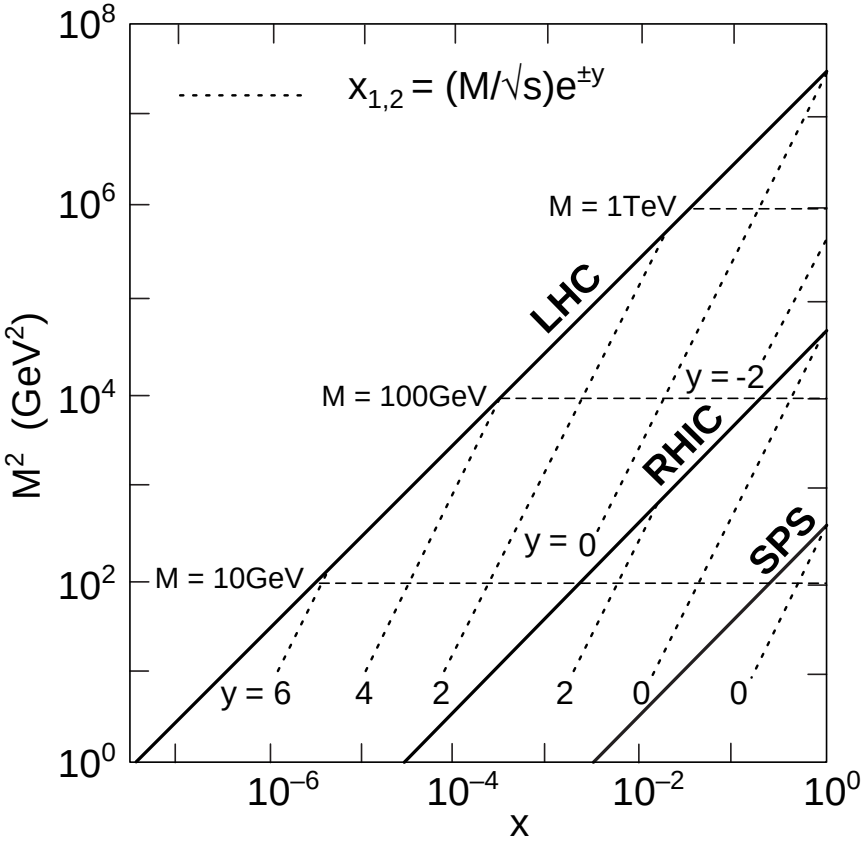

Figure 2: The Q^2 reach as a function of x for the SPS, RHIC and the LHC. Lines of constant rapidity are indicated for each machine.

Some Parameterizations of Nuclear Parton Densities

EKS98: K. J. Eskola, V. J. Kolhinen and P. V. Ruuskanen, Nucl. Phys. B 535 (1998) 351 [arXiv:hep-ph/9802350]; K. J. Eskola, V. J. Kolhinen and C. A. Salgado, Eur. Phys. J. C 9 (1999) 61 [arXiv:hep-ph/9807297].

EPS09: K. J. Eskola, H. Paukkunen and C. A. Salgado, JHEP 0904 (2009) 065 [arXiv:0902.4154 [hep-ph]].

nDS: D. de Florian and R. Sassot, Phys. Rev. D 69, 074028 (2004) [arXiv:hep-ph/0311227].

DSSZ: D. de Florian, R. Sassot, M. Stratmann and P. Zurita, Phys. Rev. D 85, 074028 (2012) [arXiv:1112.6324 [hep-ph]].

HKN: M. Hirai, S. Kumano and T. H. Nagai, Phys. Rev. C 70, 044905 (2004) [arXiv:hep-ph/0404093].

FGS10: L. Frankfurt, V. Guzey and M. Strikman, Phys. Rept. 512, 255 (2012) [arXiv:1106.2091 [hep-ph]].

EPS09s: I. Helenius, K. J. Eskola, H. Honkanen and C. A. Salgado, JHEP 1207, 073 (2012) [arXiv:1205.5359 [hep-ph]].

nCTEQ15: K. Kovarik *et al.*, Phys.Rev. D 93, 085037 (2016) [arXiv:1509.00792 [hep-ph]].

EPPS16: K. J. Eskola, P. Piakkinen, H. Paukkunen and C. A. Salgado, arXiv:1612.05741 [hep-ph].

Focus on Eskola *et al* Sets

Eskola *et al* Method Before 2016

Nuclear effects on PDFs divided into x regions

- **shadowing; a depletion at $x \lesssim 0.1$,**
- **anti-shadowing; an excess at $0.1 \lesssim x \lesssim 0.3$,**
- **EMC effect; a depletion at $0.3 \lesssim x \lesssim 0.7$**
- **Fermi motion; an excess towards $x \to 1$ and beyond.**

Define ratios of the individual and total valence and sea quark distributions and the gluon ratio in nuclei relative to protons

$$
\begin{aligned}
R^A_{\bar{q}}(x,Q^2) &\equiv \frac{\bar{q}_A(x,Q^2)}{\bar{q}(x,Q^2)} \quad R^A_{q_V}(x,Q^2) \equiv \frac{q^A_V(x,Q^2)}{q_V(x,Q^2)} \quad R^A_G(x,Q^2) \equiv \frac{g^A(x,Q^2)}{g(x,Q^2)} \\
R^A_V(x,Q^2) &\equiv \frac{u^A_V(x,Q^2) + d^A_V(x,Q^2)}{u_V(x,Q^2) + d_V(x,Q^2)}, \\
R^A_S(x,Q^2) &\equiv \frac{\bar{u}_A(x,Q^2) + \bar{d}_A(x,Q^2) + \bar{s}_A(x,Q^2)}{\bar{u}(x,Q^2) + \bar{d}(x,Q^2) + \bar{s}(x,Q^2)}
\end{aligned}
$$

Eskola *et al* Parameterizations before 2016

EPS09 fits based on piecewize functions for $i = V, S$ and G

$$R_i^A(x) = \begin{cases} a_0 + (a_1 + a_2 x)[\exp(-x) - \exp(-x_a)] & x \le x_a \\ b_0 + b_1 x + b_2 x^2 + b_3 x^3 & x_a \le x \le x_e \\ c_0 + (c_1 - c_2 x)(1-x)^{-\beta} & x_e \le x \le 1, \end{cases}$$

y_0	**Maximum shadowing effect as $x \to 0$**
x_a, y_a	**Position, height of antishadowing maximum**
x_e, y_e	**Position, height of EMC minimum**
β	**Slope in the Fermi-motion part**
$c_0 = 2y_e$	
$d_i^A = d_i^{A_C}\left(\frac{A}{A_C}\right)^{p_{d_i}}$	**A dependence of fit parameters is power law relative to $A_C = 12$**

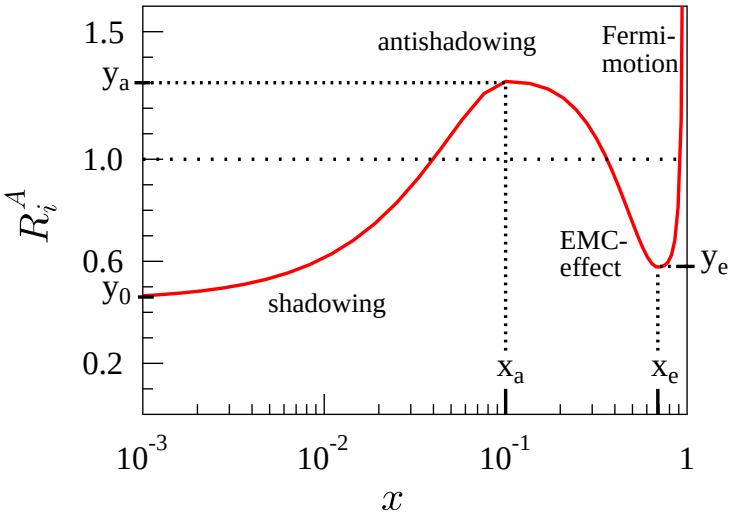

Figure 3: **An illustration of the fit function $R_i^A(x)$ and the role of the parameters x_a, x_e, y_0, y_a, and y_e.**

EPPS16

Similar division of nuclear effects on PDFs into x regions

- **shadowing; a depletion at $x \lesssim 0.1$,**
- **anti-shadowing; an excess at $0.1 \lesssim x \lesssim 0.3$,**
- **EMC effect; a depletion at $0.3 \lesssim x \lesssim 0.7$**
- **Fermi motion; an excess towards $x \to 1$ and beyond.**

Define ratios of the individual valence and sea quark distributions and the gluon ratio in nuclei relative to protons

The neutrino DIS, together with $W^{\pm}$ and Z^0 production at the LHC allows separation of the u_V and d_V as well as the $\overline{u}$ and $\overline{d}$ ratios, not possible with only the prior use of Drell-Yan data

This does, however, lead to more parameters overall, 20 instead of 15

$$
\begin{aligned}
R^A_{\bar{q}}(x,Q^2) &\equiv \frac{\bar{q}_A(x,Q^2)}{\bar{q}(x,Q^2)} \quad \bar{q} = \bar{u}, \quad \bar{d}, \quad \bar{s} \\
R^A_{q_V}(x,Q^2) &\equiv \frac{q^A_V(x,Q^2)}{q_V(x,Q^2)} \quad q_V = u_V, \quad d_v \\
R^A_G(x,Q^2) &\equiv \frac{g^A(x,Q^2)}{g(x,Q^2)}
\end{aligned}
$$

EPPS16 Parameterization

Similar parameterizations but now for $i = u_V, d_V, \overline{u}, \overline{d}, s$, and g

$$R_i^A(x) = \begin{cases} a_0 + a_1(x - x_a)^2 & x \le x_a \\ b_0 + b_1 x^\alpha + b_2 x^{2\alpha} + b_3 x^{3\alpha} & x_a \le x \le x_e \\ c_0 + (c_1 - c_2 x)(1 - x)^{-\beta} & x_e \le x \le 1, \end{cases}$$

y_0	**Maximum shadowing effect as $x \to 0$**
x_a, y_a	**Position, height of antishadowing maximum, $\alpha = 10x_a$**
x_e, y_e	**Position, height of the EMC minimum**
$\beta = 1.3$	**Slope in the Fermi-motion part**
$y_i(A) = y_i(A_C)\left(\frac{A}{A_C}\right)^{\gamma_i[y_i(A_C)-1]}$	**A dependence of fit parameters relative to $A_C = 12$**

a_i, b_i, c_i fixed from minimia and maxima at $y_0 = R_i^A(x \to 0, Q_0^2)$, $y_a = R_i^A(x_a, Q_0^2)$ and $y_e = R_i^A(x_e, Q_0^2)$, continuity and vanishing first derivatives at matching points x_a, x_e

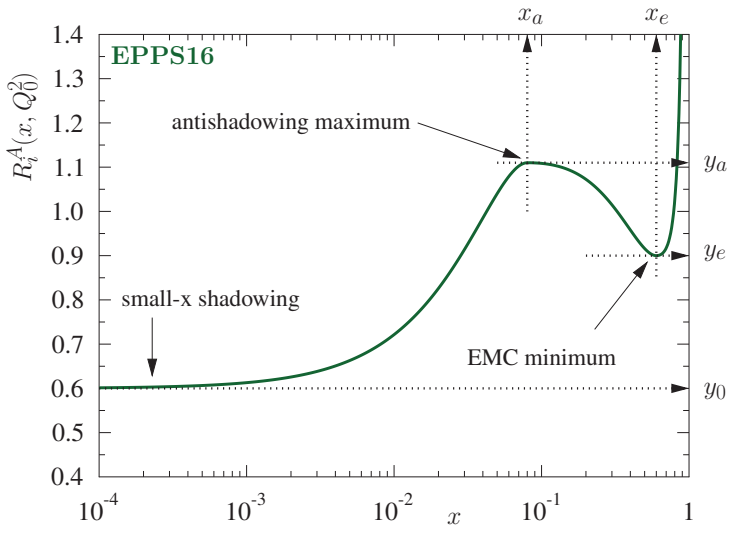

Figure 4: **An illustration of the fit function $R_i^A(x)$ and the role of the parameters x_a, x_e, y_0, y_a, and y_e.**

Differences Between Eskola *et al* Sets

EKS98: Simple parameterization for all A; leading order analysis only; GRV LO set used for proton PDFs; single set; no χ^2 analysis performed; $2.25 \leq Q^2 \leq 10^4$ GeV^2; $10^{-6} < x < 1$

EPS08: Simple parameterization for all A; leading order analysis only; CTEQ61L set used for proton PDFs; single set; χ^2 analysis uses forward BRAHMS data from RHIC to maximize gluon shadowing; $1.69 \leq Q^2 \leq 10^6$ GeV^2; $10^{-6} < x < 1$

EPS09: Available for only some specific values of A; LO and NLO sets available based on CTEQ61L and CTEQ6M respectively; χ^2 analysis done at both LO and NLO; calling routine similar to other sets but now there are 31, 15 above and 15 below the central set; no longer use BRAHMS data

EPPS16: For the first time, used neutrino DIS and LHC gauge boson and dijet data; use general mass formalism for generating heavy flavor, SACOT; undo experimental isospin corrections in DIS data to have "isoscalar targets"; NLO set only based on CT14NLO; $Q_0^2 = 1.69$ GeV^2

In all cases, when A, x or Q^2 are outside the range of validity, the last value is returned, *e.g.* if $x < 10^{-6}$ value at $x = 10^{-6}$ is given (I believe this is still true for EPPS16, the sets will not be available until after paper is published)

Data Included in EPPS16 Fits (Inclusive of Prior Fits)

Total number of points included, 1811, total χ^2 is 1789

Data sets sorted by mass of heaviest target

CDHSW and NuTeV data not used because no correlations of systematic uncertainties available, CHORUS Pb target has larger neutron excess than Fe so gives more information on flavor separation

For π beams, used GRV pion PDFs

Experiment	Process	Collisions	# points	χ^2
SLAC E139	DIS	e^-He, e^-D	21	12.2
CERN NMC 95, re.	DIS	μ^-He, μ^-D	16	18.4
CERN NMC 95	DIS	μ^-Li, μ^-D	15	18.4
CERN NMC 95, Q^2 dep.	DIS	μ^-Li, μ^-D	153	161.2
SLAC E139	DIS	e^-Be, e^-D	20	12.9
CERN NMC 96	DIS	μ^-Be, μ^-C	15	4.4
SLAC E139	DIS	e^-C, e^-D	7	6.4
CERN NMC 95	DIS	μ^-C, μ^-D	15	9.0
CERN NMC 95, Q^2 dep.	DIS	μ^-C, μ^-D	165	133.6
CERN NMC 95, re.	DIS	μ^-C, μ^-D	16	16.7
CERN NMC 95, re.	DIS	μ^-C, μ^-Li	20	27.9
FNAL E772	DY	pC, pD	9	11.3
SLAC E139	DIS	e^-Al, e^-D	20	13.7
CERN NMC 96	DIS	μ^-Al, μ^-C	15	5.6
SLAC E139	DIS	e^-Ca, e^-D	7	4.8
FNAL E772	DY	pCa, pD	9	3.33
CERN NMC 95, re.	DIS	μ^-Ca, μ^-D	15	27.6
CERN NMC 95, re.	DIS	μ^-Ca, μ^-Li	20	19.5
CERN NMC 96	DIS	μ^-Ca, μ^-C	15	6.4

Experiment	Process	Collisions	# points	χ^2
SLAC E139	DIS	e^-Fe, e^-D	26	22.6
FNAL E772	DY	pFe, pD	9	3.0
CERN NMC 96	DIS	μ^-Fe, μ^-C	15	10.8
FNAL E866	DY	pFe, pBe	28	20.1
CERN EMC	DIS	μ^-Cu, μ^-D	19	15.4
SLAC E139	DIS	e^-Ag, e^-D	7	8.0
CERN NMC 96	DIS	μ^-Sn, μ^-C	15	12.5
CERN NMC 96, Q^2 dep.	DIS	μ^-Sn, μ^-C	144	87.6
FNAL E772	DY	pW, pD	9	7.2
FNAL E866	DY	pW, pBe	28	26.1
CERN NA10*	DY	π^-W, π^-D	10	11.6
FNAL E615*	DY	π^+W, π^-W	11	10.2
CERN NA3*	DY	π^-Pt, π^-H	7	4.6
SLAC E139	DIS	e^-Au, e^-D	21	8.4
RHIC PHENIX	π^0	dAu, pp	20	6.9
CERN NMC 96	DIS	μ^-Pb, μ^-C	15	4.1
CERN CMS*	$W^\pm$	pPb	10	8.8
CERN CMS*	Z^0	pPb	6	5.8
CERN ATLAS*	Z^0	pPb	7	9.6
CERN CMS*	dijet	pPb	7	5.5
CERN CHORUS*	DIS	νPb, $\overline{\nu}$Pb	824	998.6

Table 1: **The data sets used in the analyses. The reactions are given for each specific case. The number of data points given are only those that satisfy the kinematic cuts, $Q^2, M^2 \geq 1.69\,\mathrm{GeV}^2$ for DIS and DY, and $p_T \geq 2\,\mathrm{GeV}$ for hadron production at RHIC. Only these points contribute to the χ^2 of each set. The data added since the EPS09 analysis are marked with a star. Eskola *et al*, arXiv:1612.05741 [hep-ph].**

Comparison of x, Q^2 Ranges of EPS09NLO and EPPS16

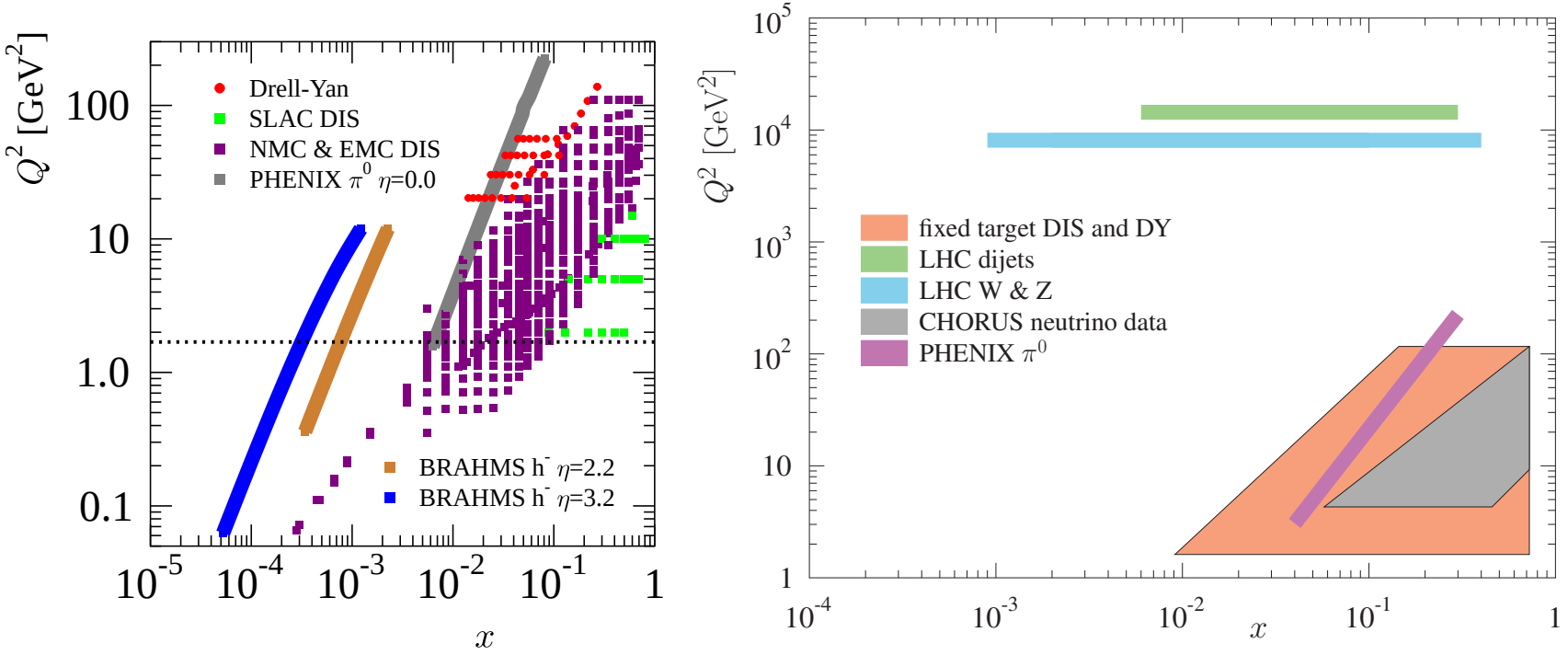

Figure 5: **Left: Data included for EPS09, JHEP 0904 (2009) 065. Right: Data included for EPPS16. Eskola *et al*, arXiv:1612.05741 [hep-ph].**

EPS09 Fitting Procedure

Define a local χ^2 based on N data sets and a given input parameter set to be varied, $\{a\}$, with χ^2_N for each data set

Set of weight factors w_N used to amplify the importance of χ^2_N to the fit for sets that have large influence but small relative χ^2

$$\chi^2(\{a\}) \equiv \sum_N w_N \chi^2_N(\{a\})$$

$$\chi^2_N(\{a\}) \equiv \left(\frac{1-f_N}{\sigma_N^{\rm norm}}\right)^2 + \sum_{i\in N}\left[\frac{f_N D_i - T_i(\{a\})}{\sigma_i}\right]^2,$$

D_i are data points with a σ_i point-to-point uncertainty (statistical and systematic uncertainties added in quadrature), f_N is normalization factor for sets with relative normalization uncertainty $\sigma_N^{\rm norm}$ fixed each iteration by minimizing χ^2_N for each parameter set $\{a\}$, T_i is calculated value to be compared to $f_N D_i$

Weak constraint on low x gluons so to cure unwanted parameter drift into unphysical region with stronger shadowing at small A, introduce penalty

$$1000\left[\left(y_0^G({\rm He}) - y_0^G({\rm Pb})\right) - \left(y_0^S({\rm He}) - y_0^S({\rm Pb})\right)\right]^2$$

If χ^2-minimized set of parameters, $\{a_0\}$, gives best estimate of nPDFs, work in a basis $\{z\}$ that diagonializes covariance matrix, errors in nPDFs computed within 90% confidence criteria, $\Delta\chi^2 = 50$

Upper and lower uncertainties on observable X computed using prescription

$$(\Delta X^+)^2 \approx \sum_k \left[\max\left\{X(S_k^+) - X(S^0), X(S_k^-) - X(S^0), 0\right\}\right]^2$$

$$(\Delta X^-)^2 \approx \sum_k \left[\max\left\{X(S^0) - X(S_k^+), X(S^0) - X(S_k^-), 0\right\}\right]^2$$

EPPS16 Fitting Procedure

Similar Hessian method to EPS09 but with some notable differences

Define a local χ^2 based on N data sets and a given input parameter set to be varied, $\{a\}$, χ^2_N

No longer require weight factors to amplify the importance of certain data sets

$$\chi^2(\{a\}) \equiv \sum_N \chi^2_N(\{a\})$$

$$\chi^2_N(\{a\}) \equiv \left(\frac{1-f_N}{\sigma_N^{\rm norm}}\right)^2 + \sum_{i\in N}\left[\frac{f_N D_i - T_i(\{a\})}{\sigma_i}\right]^2,$$

D_i are data points with a σ_i point-to-point uncertainty (statistical and systematic uncertainties added in quadrature), f_N is normalization factor for sets with relative normalization uncertainty $\sigma_N^{\rm norm}$ fixed each iteration by minimizing χ^2_N for each parameter set $\{a\}$, T_i is calculated value to be compared to $f_N D_i$

No longer require penalty terms to avoid regions where small A nuclei have larger effects because of the way A dependence is incorporated into parameters

Do introduce a penalty term at low x if $F_L^A < 0$ but results are not sensitive to requirement

In this case, confidence criteria is $\Delta\chi^2 = 52$

Upper and lower uncertainties in any observable X can be computed using same prescription as EPS09 but now 41 total sets instead of 31, increases width of uncertainty bands

Results for Eskola *et al* Sets

Q^2 Dependence of EPS09

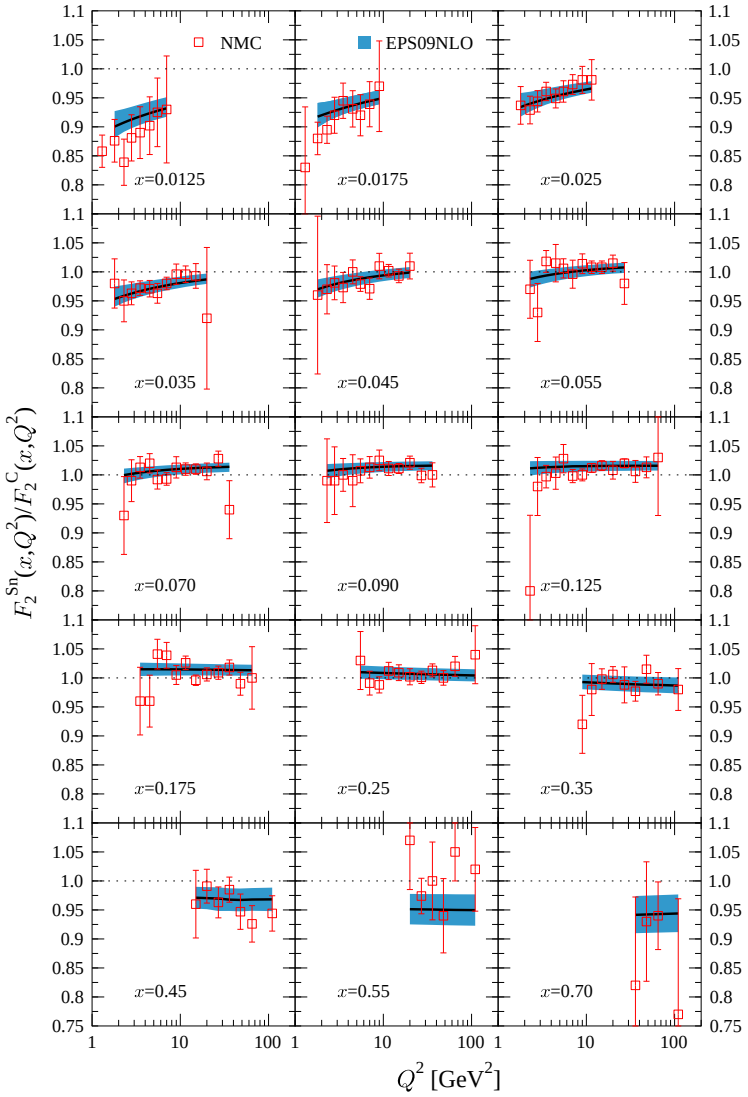

Figure 6: **Evolution of $F_2^{\mathrm{Sn}}/F_2^{\mathrm{C}}$ with Q^2 for different values of x with EPS09 NLO, JHEP 0904 (2009) 065.**

x Dependence of EPS09 NLO

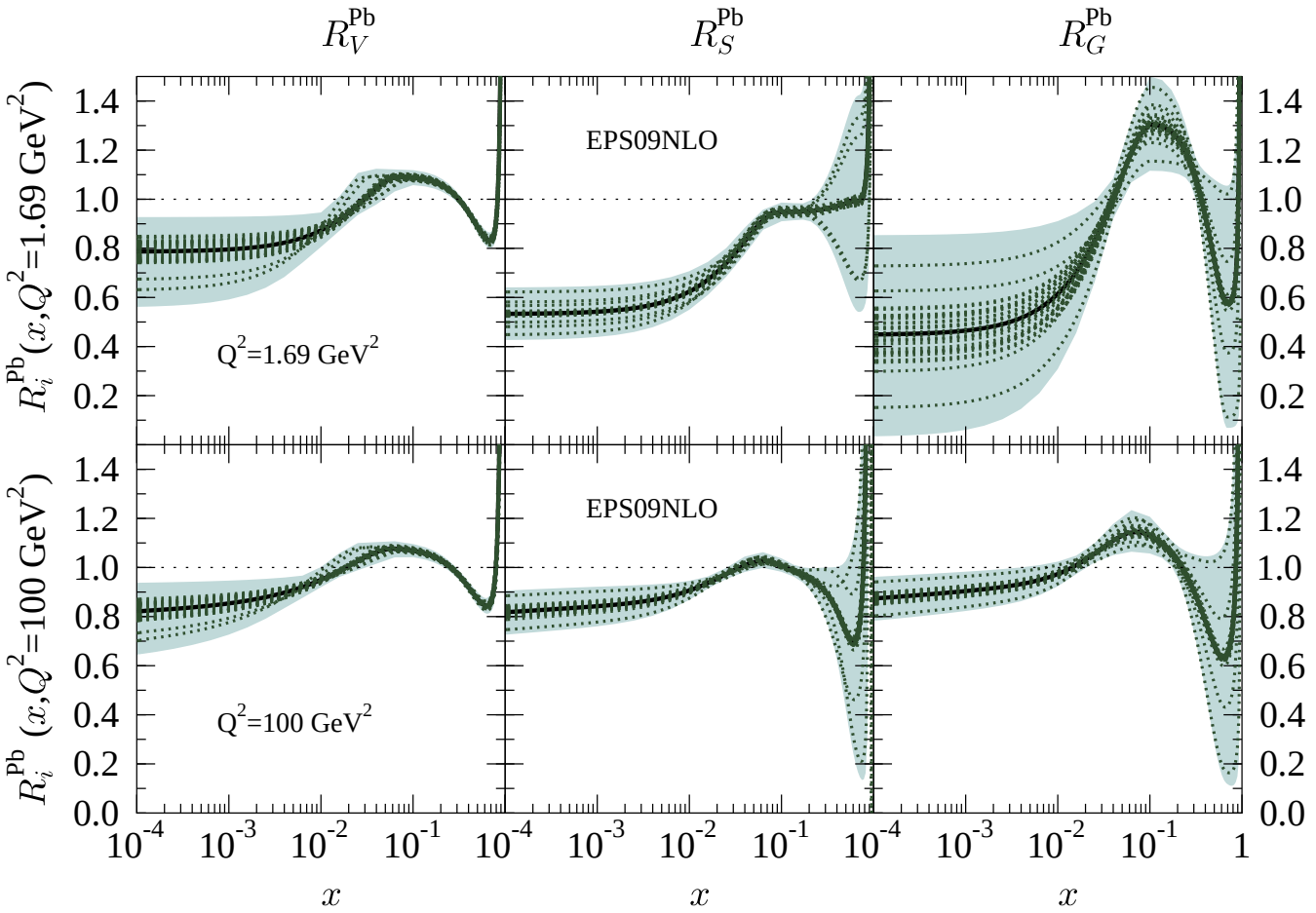

Figure 7: **The x dependence of the valence (left), sea (center), and gluon (right) distributions for the starting scale $Q^2 = 1.69$ GeV^2 (top) and $Q^2 = 100$ GeV^2 (bottom), JHEP 0904 (2009) 065.**

Q^2 Dependence of EPPS16

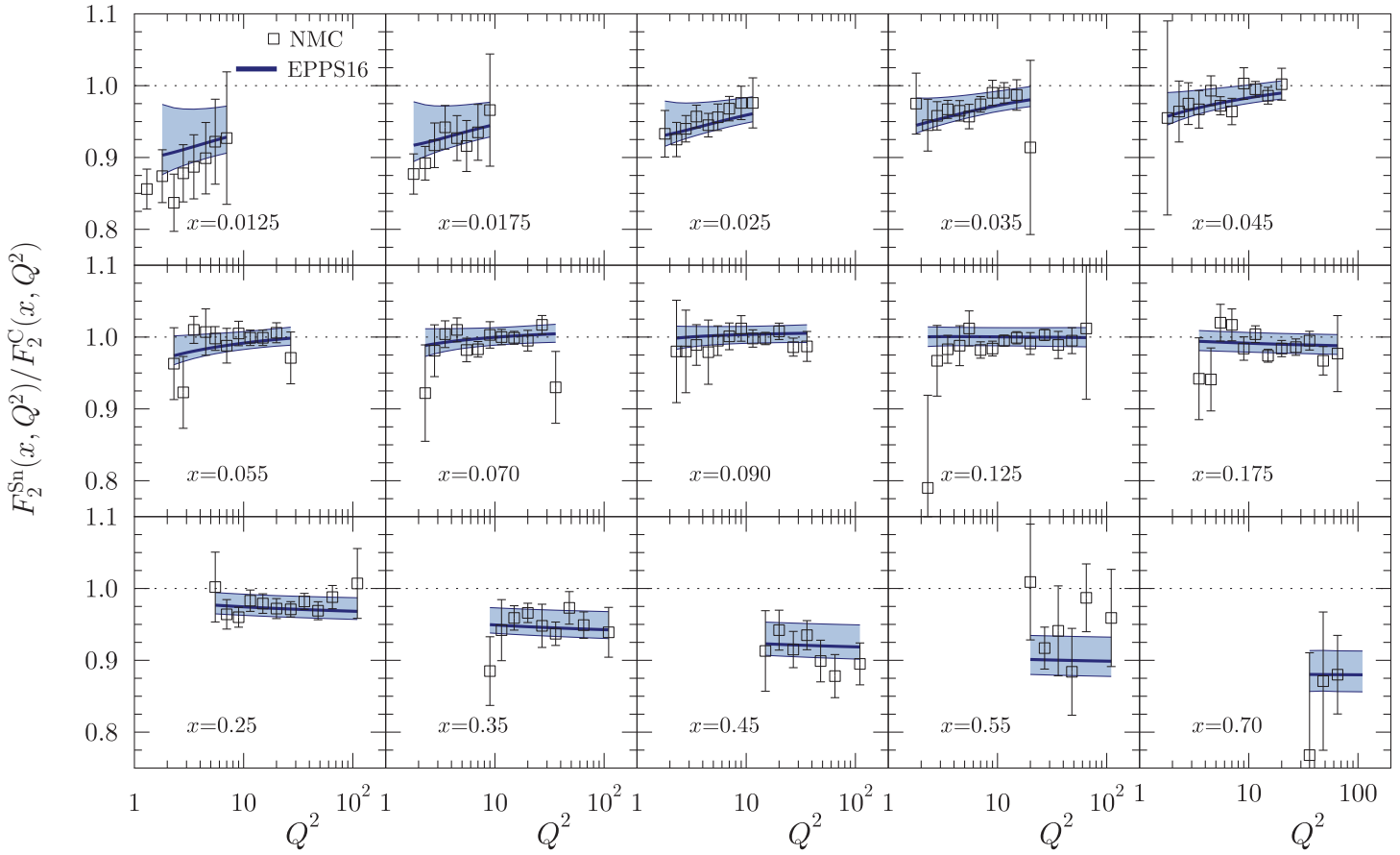

Figure 8: **Evolution of $F_2^{\mathrm{Sn}}/F_2^{\mathrm{C}}$ with Q^2 for different values of x with EPPS16. Eskola *et al*, arXiv:1612.05741 [hep-ph].**

x Dependence of EPPS16

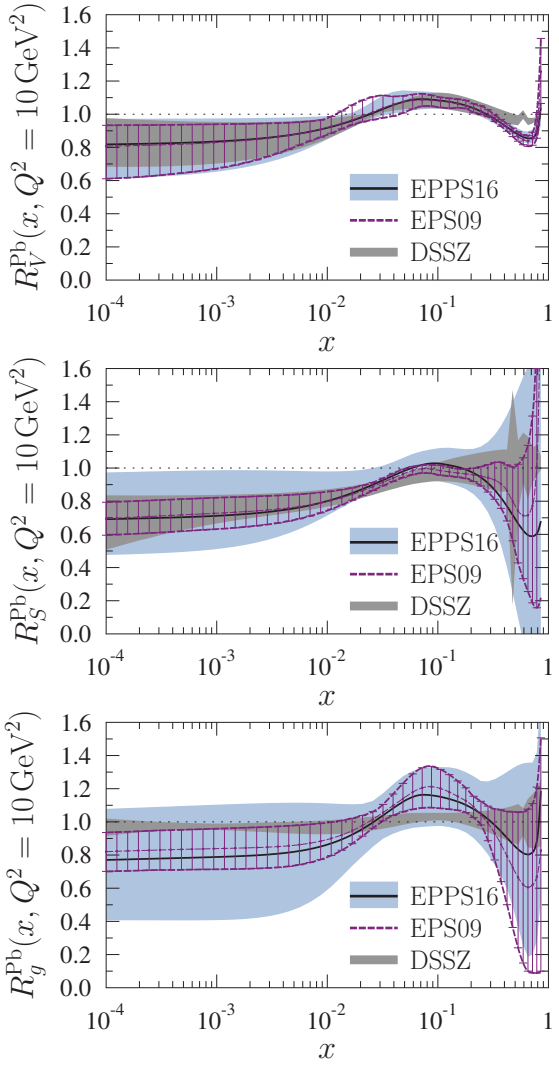

Figure 9: **The x dependence of the average valence (left), sea (center), and gluon (right) distributions for $Q^2 = 10$ GeV^2. EPPS16 (blue-gray band) is compared to EPS09NLO (red band) and DSSZ (dark-gray band). Eskola *et al*, arXiv:1612.05741 [hep-ph].**

Centrality Dependence of Nuclear Modifications

Impact Parameter Dependence of EPS09s

Previous impact-parameter dependent EPS09 calculations (RV and S Klein) were based on linear dependence on nuclear profile function $T_A(s)$

EPS09s (and EKS98s) sets taken as input to b-dependent calculation and assuming shadowing depends on $T_A(b)$, sum up to quartic terms in $T_A(b)$ to get A-independent coefficients

Result is somewhat similar to dependence of FGS10 but both are weaker than PHENIX J/ψ data

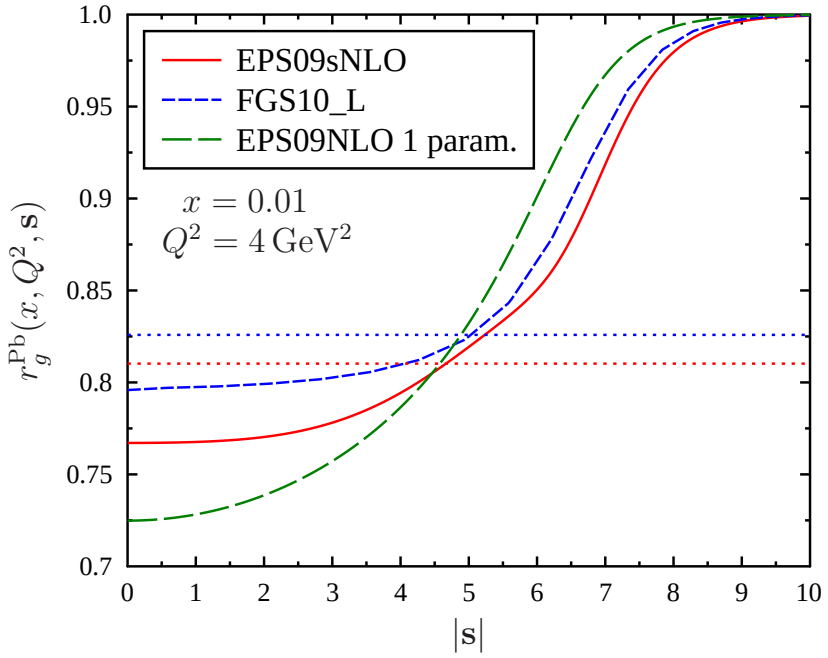

Figure 10: **Comparison of the spatial dependence of the gluon modification in a lead nucleus, $r_g^{\mathrm{Pb}}(x, Q^2, s)$, between FGS10_L (short-dashed blue curves), 1-parameter approach (long-dashed green) and our spatial fits (solid red) EPS09sNLO1. The scale $Q^2 = 4$ GeV^2 for all plots but the values of x have been chosen so that the spatially averaged $R_g^{\mathrm{Pb}}(x, Q^2)$ (dotted horizontal red lines) approximately coincides with FGS10_L (dotted blue). Helenius *et al.*, JHEP 1207 (2012) 073.**

Centrality Dependence of Shadowing – Test with J/ψ

RHIC minimum bias (impact-parameter integrated shadowing) d+Au data agrees with EPS09 shadowing and 4 mb absorption cross section

The R_{CP} ratio does not agree with the impact-parameter dependent shadowing calculation at forward rapidity because the peripheral result is overestimated

Correlation between uncertainties allows

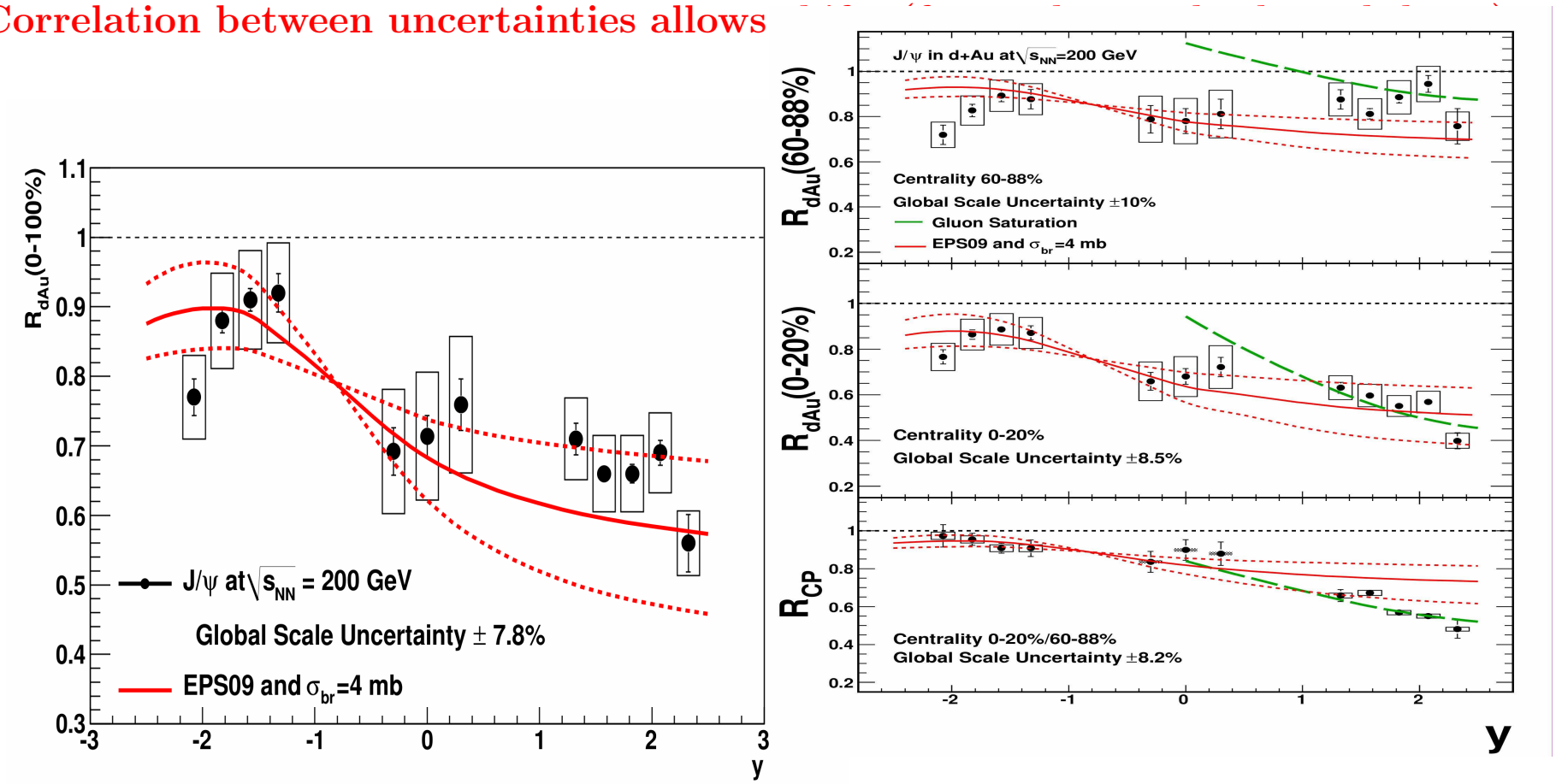

Figure 11: The PHENIX data compared to calculations of EPS09 shadowing including uncertainties and a constant absorption cross section of 4 mb. Left: the minimum bias result. Right: Including impact-parameter dependent shadowing in the $60-88\%$ centrality (top) and $0-20\%$ centrality (middle) bins. The lower panel shows the central-to-peripheral ratio. The dashed curves shows a gluon saturation calculation. PHENIX, Phys. Rev. Lett. **107** (2011) 142301.

Is Shadowing Concentrated in the Nuclear Core?

Onset of shadowing with impact parameter r_T consistent with shadowing effects concentrated in core of nucleus where nucleons are more densely packed

Used fit function with $M_{\rm shad} = 1 - (1 - R_g(x,Q^2))/(a(R,d)(1+\exp((r_T - R)/d)))$ where $a(R,d)$ is adjusted to give the average $R_g(x,Q^2)$, found $R = 2.4$ fm and $d = 0.12$ fm, shadowing much stronger function of b than either EPS09s or FGS10

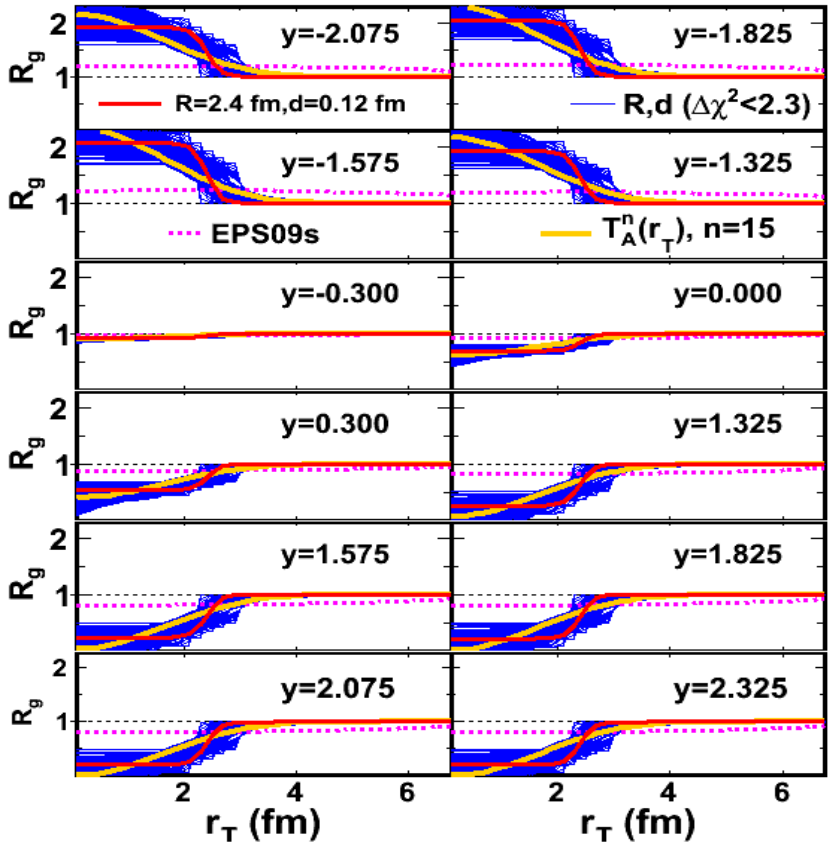

Figure 12: (Left) The gluon modification from the best fit global R and d (solid red line), along with results for all combinations of R and d within the $\Delta\chi^2 = 2.3$ fit contour (thin blue lines). The modification from $T_A^n(r_T)$ ($n = 15$) is shown by the solid orange line. The dashed magenta line is the EPS09s impact parameter dependence. [D. McGlinchey, A. D. Frawley and RV, Phys. Rev. C **87** (2013) 054910.]

Predictions for Several Final States

Dijets in CMS at 5.02 TeV

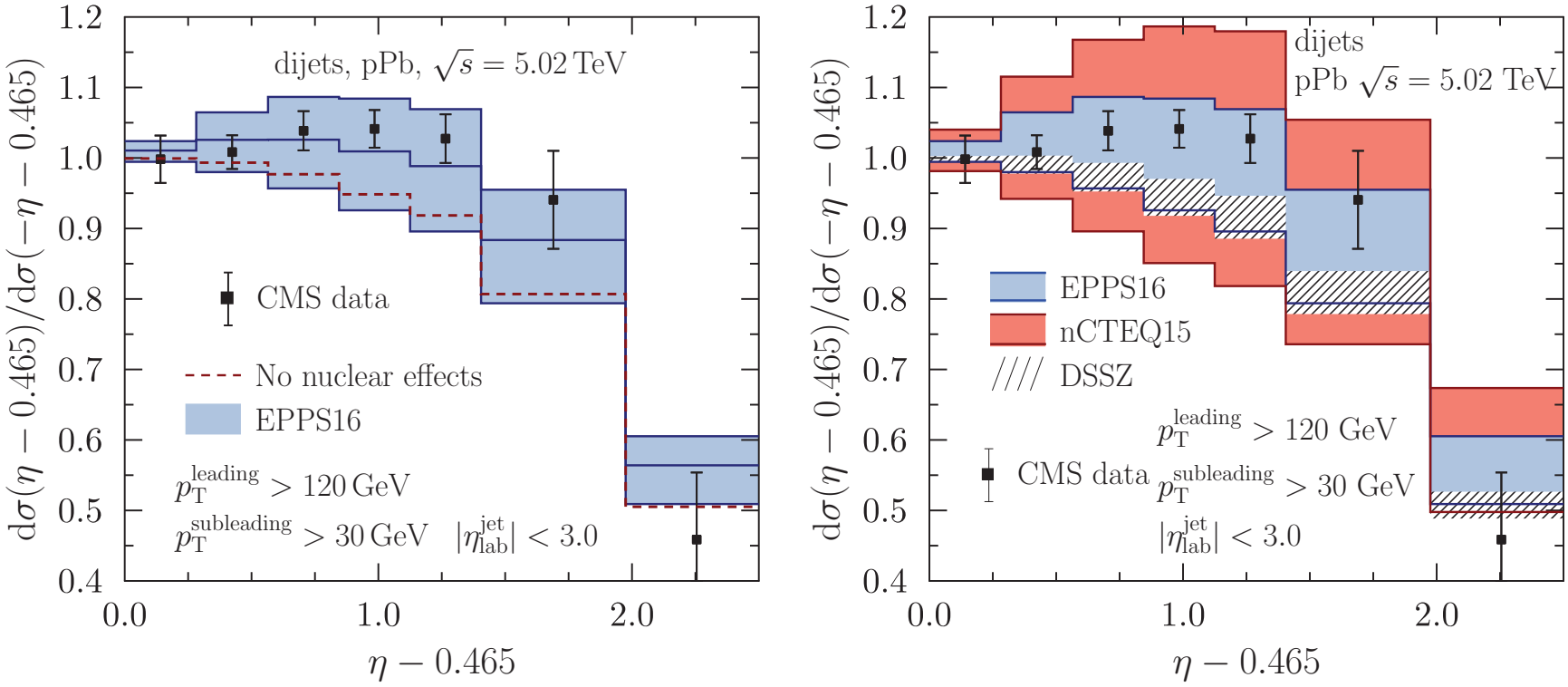

Figure 13: **Left: Dijet production with EPPS16 compared to no nuclear effects, isospin only. Right: EPPS16 results are compared to nCTEQ and DSSZ. Eskola *et al*, arXiv:1612.05741 [hep-ph].**

Asymmetries in W^+, W^- production in CMS at 5.02 TeV

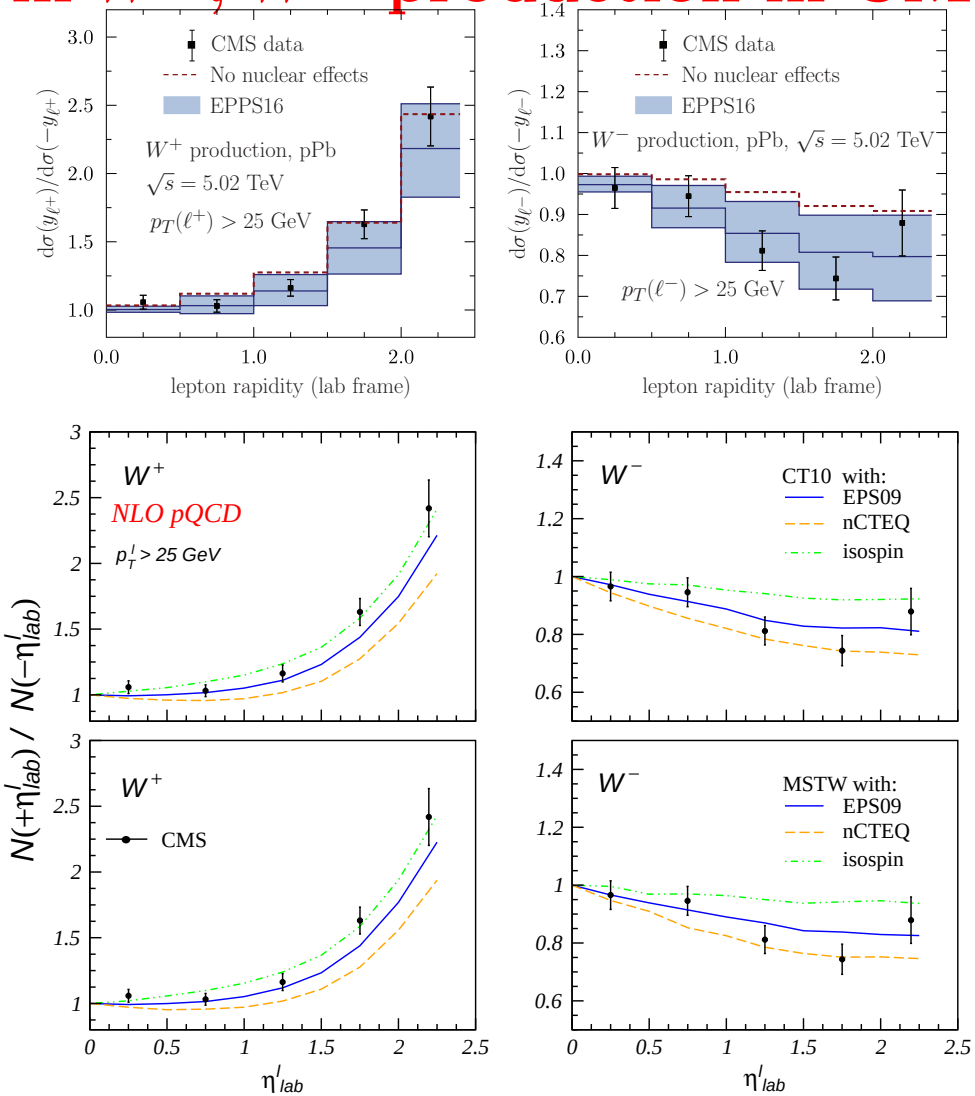

Figure 14: **Top: Lepton forward-backward asymmetry for W^+ (left) and W^- (right) with EPPS16. Eskola *et al*, arXiv:1612.05741 [hep-ph]. Bottom: Calculation by BW Zhang *et al.* in Albacete *et al.*, Int. J. Mod. Phys. E 25 (2016) 1630005.**

Z^0 Forward-Backward Asymmetry at 5.02 TeV

The forward-backward asymmetry for CMS, near midrapidity, is well reproduced

The LHCb data, at higher rapidity, are not well reproduced at backward rapidity but very few events and y limits for asymmetry reduce yield further

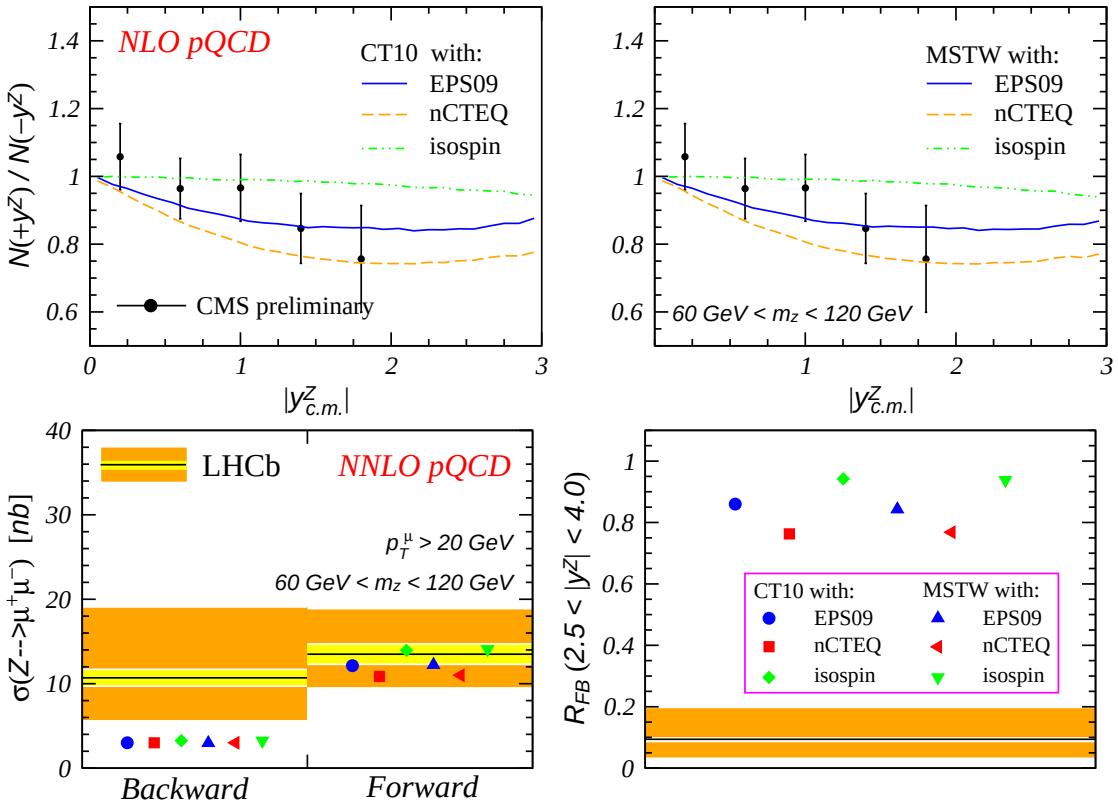

Figure 15: The forward-backward asymmetry, as a function of the absolute value of Z^0 rapidity in the center of mass frame in p+Pb collisions at $\sqrt{s_{NN}} = 5.02$ TeV. (Top) The results with the CT10 (left) and MSTW2008 PDFs (right) are shown with the CMS data (Nucl. Phys. A **931** (2014) 718). (Bottom) The forward and backward cross sections (left) and forward-backward asymmetry (right) for Z^0 production in LHCb (JHEP **1409** (2014) 030). Calculation by BW Zhang *et al.* in Albacete *et al.*, Int. J. Mod. Phys. E **25** (2016) 1630005.

Predictions for Quarkonium $R_{p\mathrm{Pb}}(y)$

EKS98 LO follows EPS09 NLO central set until $y > -2$ where it decreases linearly while EPS09 becomes flatter, central EPPS16 should be like EPS09NLO

EPS09 abrupt change of slope near antishadowing region follows from the gluon shadowing ratio, almost like the low x behavior had to join to assumed antishadowing shape at intermediate x

nDS and nDSg, with no antishadowing, have a weaker y dependence overall

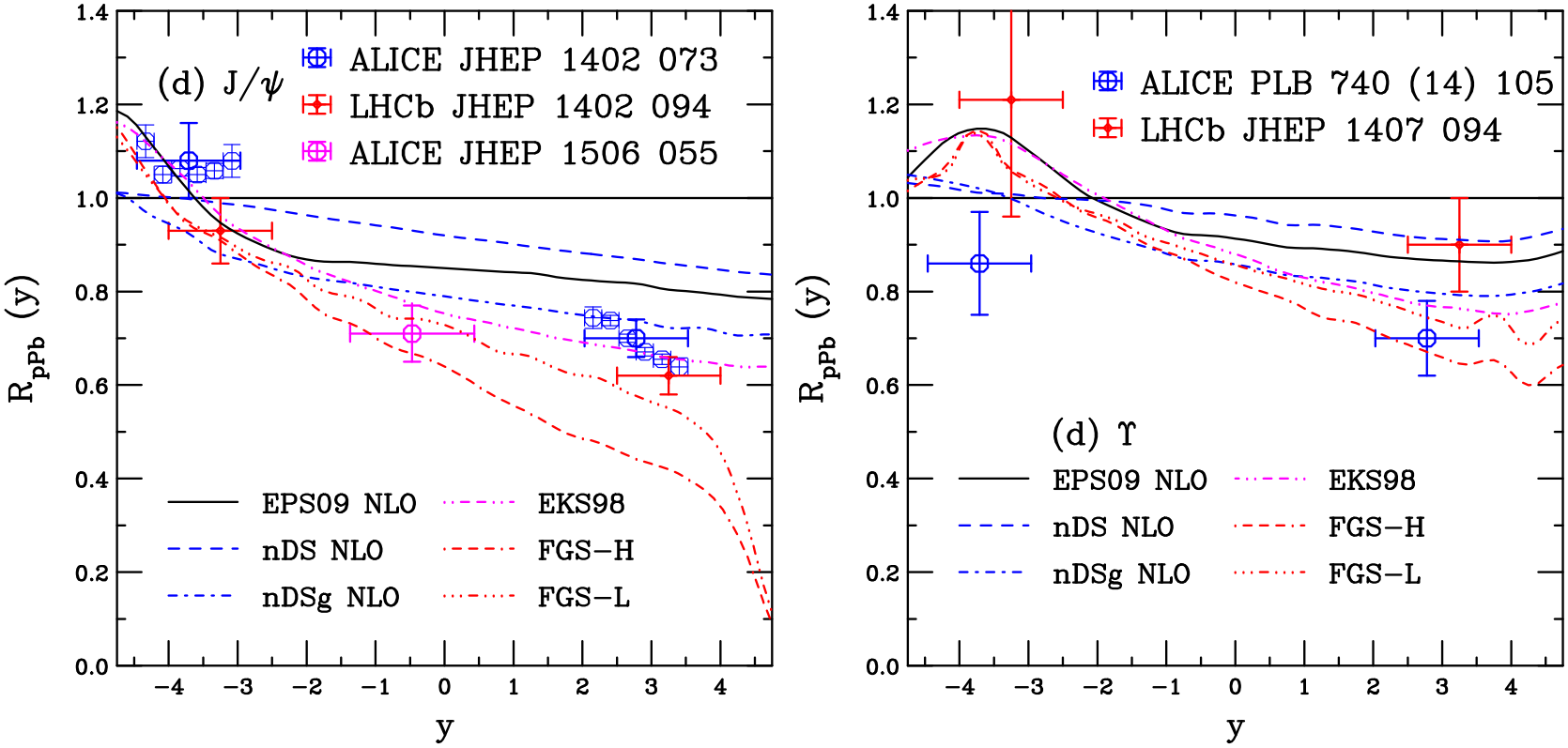

Figure 16: **The calculated $R_{p\mathrm{Pb}}(y)$ for J/ψ (left) and Υ (right) with central EPS09 NLO (black), nDS NLO (blue), nDSg NLO (red) and EKS98 LO (magenta). RV, Phys. Rev. C 92 (2015) 034909.**

NLO vs LO EPS09, J/ψ and Υ

The nPDF set should be appropriate to the order of the calculation: if using the LO set in a NLO calculation agrees better with the data, it isn't really better

NLO calculation required for CEM p_T distribution and is more appropriate

LO CEM uncertainty band is broader, with stronger shadowing, to counterbalance the flatter low x behavior of CTEQ61L while CTEQ6M is valence-like: different behavior of proton PDFs makes good order-by-order agreement of $R_{p\mathrm{Pb}}$ difficult

Starting scale of EPS09 is 1.69 GeV^2, same as CTEQ6 starting scale

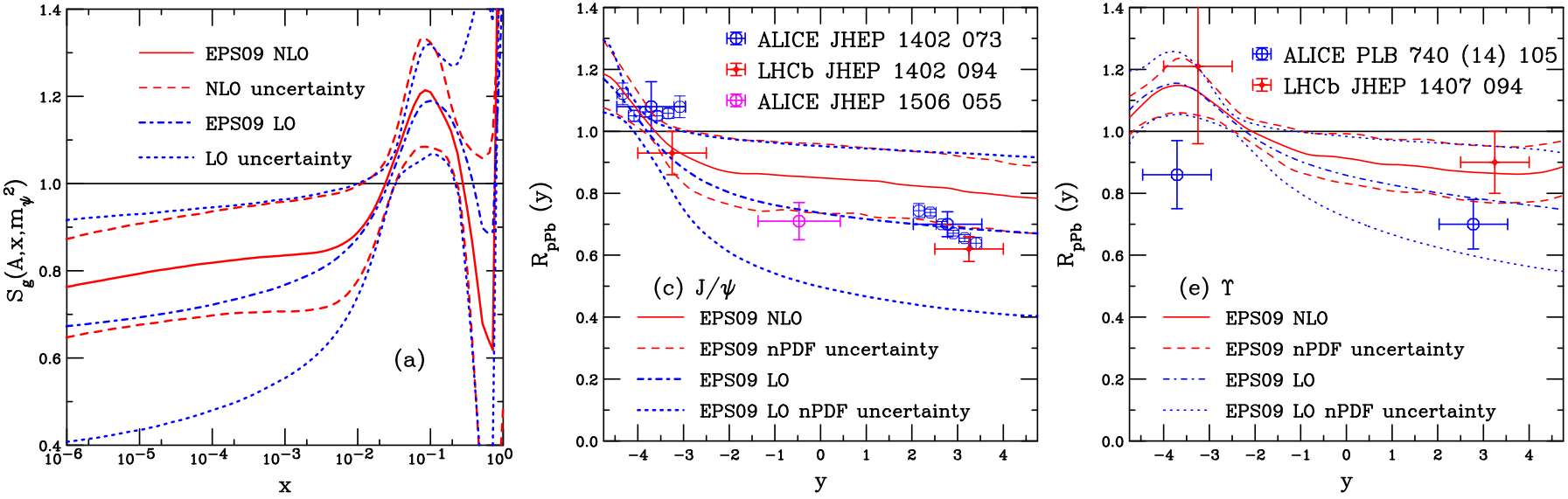

Figure 17: **(Left) The EPS09 LO (blue) and NLO (red) uncertainty bands for gluon shadowing. The corresponding uncertainty bands for $R_{p\mathrm{Pb}}(y)$ at $\sqrt{s_{NN}} = 5$ TeV for J/ψ (center) and Υ (right). RV, Phys. Rev. C 92 (2015) 034909.**

NLO vs LO nDS, J/ψ and Υ

While there are some differences between the LO and NLO nDS and nDSg ratios, especially for nDSg at $x \sim 0.01$, the LO and NLO ratios are much closer than those of the EPS09 central sets, here order of calculation is not an issue

nDS(g) employs GRV98 LO and NLO proton PDFs, the Q^2 range of the nPDF, $1 < Q^2 < 10^6$ GeV^2, is above the minimum scale of GRV98, unlike EPS09 and CTEQ6

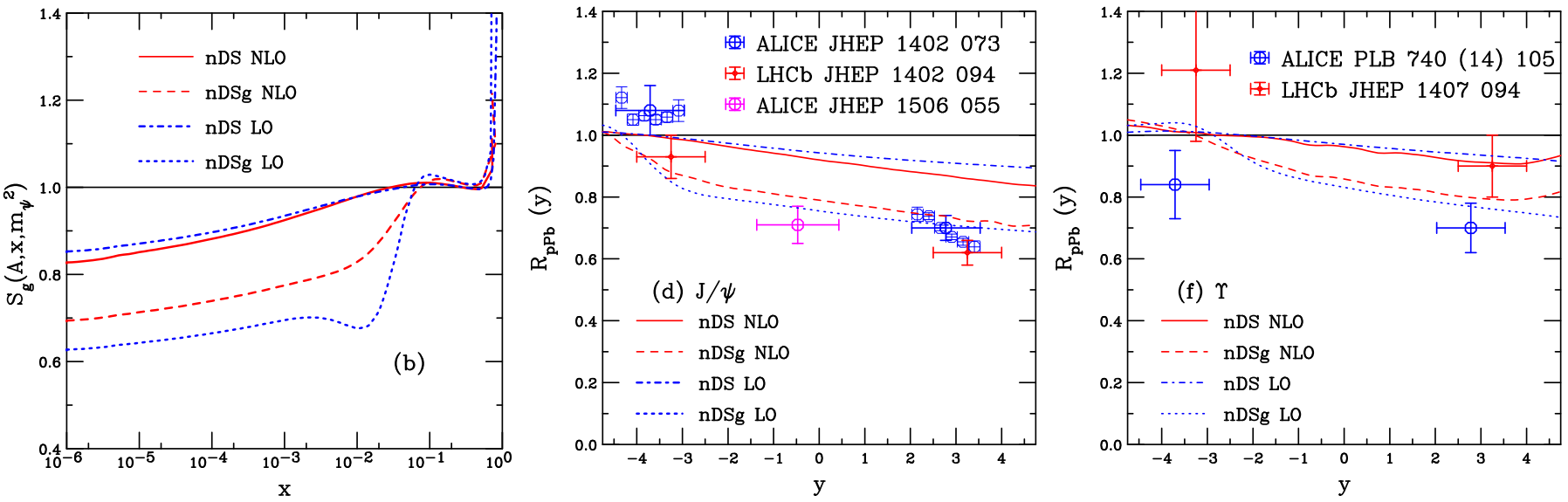

Figure 18: **(Left) The nDS and nDSg LO (blue) and NLO (red) gluon shadowing ratios. The corresponding results for $R_{\rm pPb}(y)$ at $\sqrt{s_{NN}} = 5$ TeV are shown for J/ψ (center) and Υ (right). RV, Phys. Rev. C 92 (2015) 034909.**

Predictions for Heavy Flavor at 8 TeV

Calculations based on data driven parameterization of open heavy flavor and quarkonium production by Shao and Lansberg compare nPDF predictions for D^0 and B^+ production

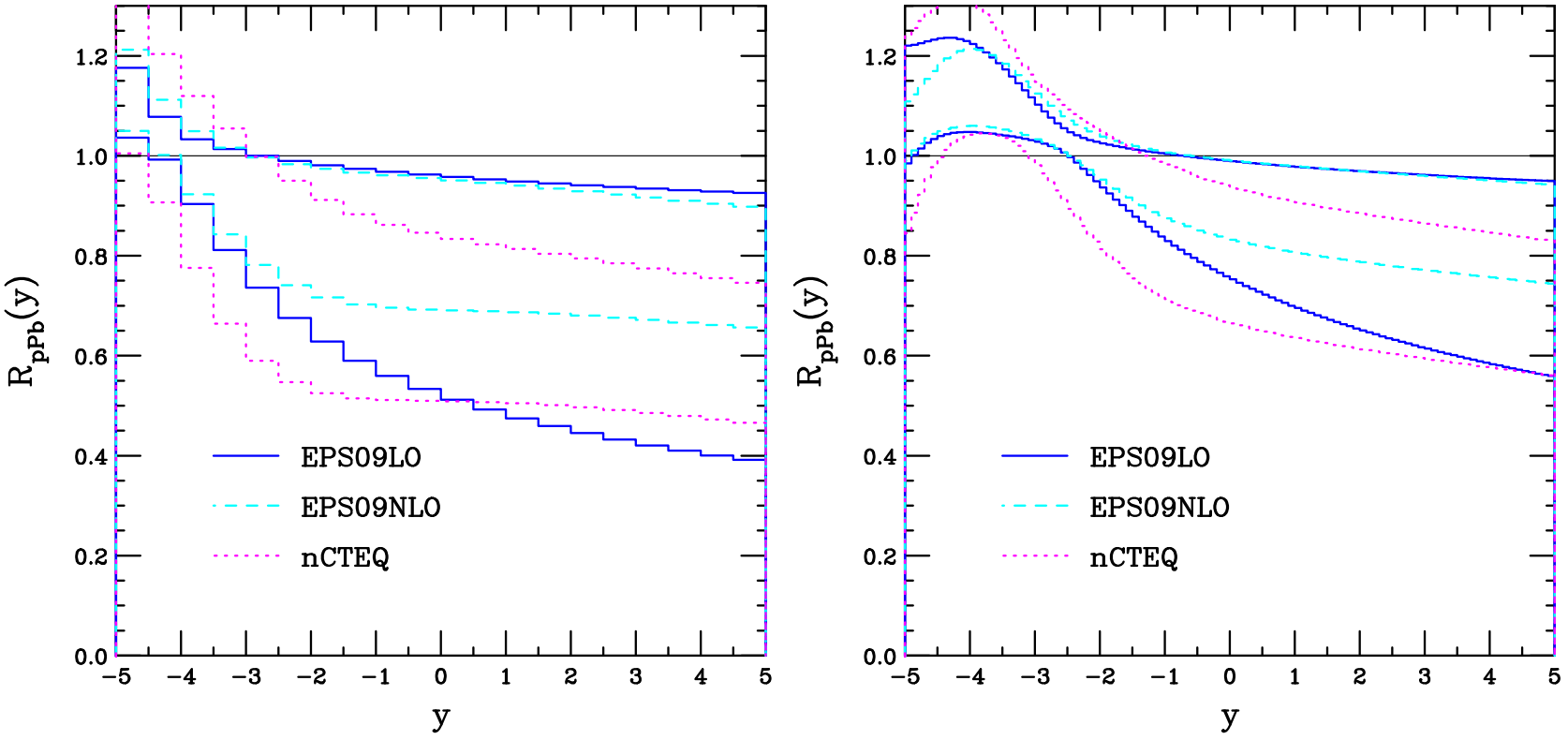

Figure 19: **The calculated $R_{p\mathrm{Pb}}(y)$ for D^0 (left) and B^+ (right) with EPS09 LO (blue), EPS09 NLO (cyan) and nCTEQ (red). Albacete *et al.*, in preparation.**

Predictions for Drell-Yan at 8 TeV

Nuclear effects on Drell-Yan production at 8 TeV, calculated at NLO by Arleo and collaborators

Isospin effect small away from antishadowing region where x is smaller and differences between nPDF effects on quark distributions small

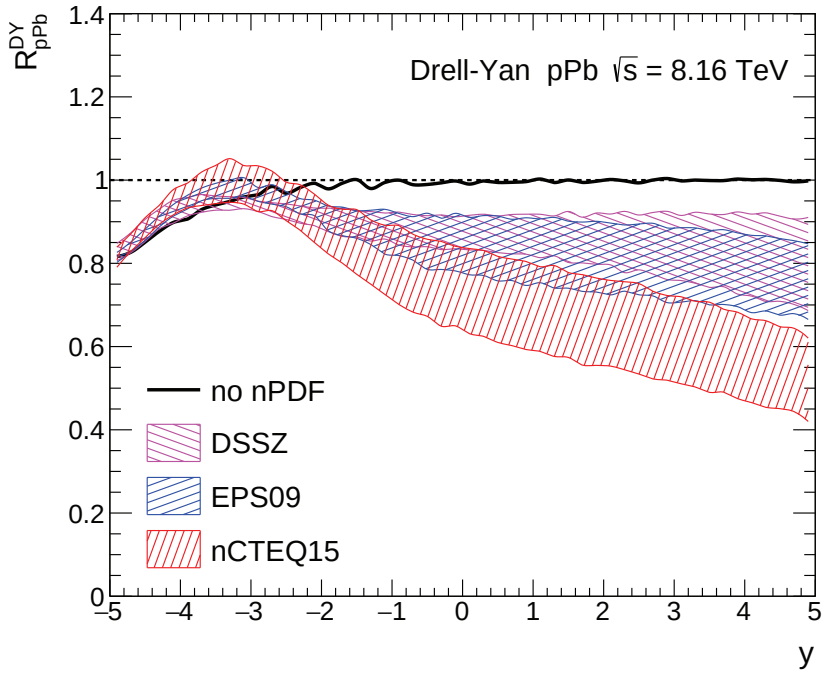

Figure 20: **The calculated $R_{p\mathrm{Pb}}(y)$ for Drell-Yan production with EPS09 NLO (blue), DSSZ (magenta), and nCTEQ16 (red). Albacete *et al.*, in preparation.**

Summary

- **Latest set by Eskola and collaborators is the first to incorporate LHC p+Pb data, finally entering a regime where x can be low and Q^2 is high**
- **Interestingly, the central result for the EKS98 and EPS09LO as well as EPS09NLO and EPPS16 does not change much, only uncertainties change**
- **Flavor separation is now possible but gluon is still not probed directly, photonuclear processes offer more direct probe**
- **Differences in nPDF analyses lead to different predictions for observables, uncertainties still large, especially for gluon**